Adsorption of CO_2 on oxidized, defected, hydrogen and oxygen covered rutile (1 × 1)-TiO_2(110)

S. Funk and U. Burghaus*

Received 11th July 2006, Accepted 5th September 2006
First published as an Advance Article on the web 14th September 2006
DOI: 10.1039/b609768e

Presented are initial, S_0 and coverage, Θ, dependent S(Θ), adsorption probability measurements of CO_2 as a function of impact energy, E_i = 0.12–1.3 eV, adsorption temperature, T_s = 85–300 K, hydrogen and oxygen pre-exposure, as well as density of defects, Γ, as varied by annealing (T = 600–900 K) and Ar^+ ion sputtering (dose χ_{Ar} at 600 eV at 85 K) of a rutile (1 × 1) TiO_2(110) surface. The defect densities were qualitatively characterized by thermal desorption spectroscopy (TDS) of CO_2. The CO_2 TDS curves consisted of two structures that can be assigned to adsorption on pristine and oxygen vacancy sites, in agreement with earlier studies. S_0 decreased linearly with E_i and was independent of T_s. The adsorption dynamics were dominated by the effect of precursor states leading to Kisliuk-like shapes over the E_i and T_s range studied. Oxygen vacancy sites reduced S_0 of CO_2. Preadsorbed oxygen blocked preferentially defect sites, which led to an increase in S_0. Hydrogen preadsorption results in physical site blocking with decreased S_0 as H-preexposure increased, while the shape of S(Θ) curves was conserved. In contrast to oxygen, hydrogen does not adsorb preferentially on defect sites. The adsorption probability data were parameterized by analytic functions (Kisliuk model) and by Monte Carlo simulations (MCSs).

1. Introduction

A large number of applications in catalysis and material science are known for TiO_2-based systems which justify investigations of gas-surface adsorption dynamics and kinetics since the adsorption of gas-phase species is the first step in all heterogeneously catalytic reactions. For example, Au–TiO_2 is a low temperature CO oxidation[1] and PROX[2] (preferential oxidation of CO in the presence of excess hydrogen)-catalyst. TiO_2 was used in photocatalysis,[3,4] as a protective coating,[5] as a biocompatible material,[6] for solar[7] and fuel[2] cells, for propylene epoxidation,[2] as a sensor,[8] and as a component of batteries.[9] Furthermore, TiO_2 developed into a prototype system for surface science studies on model catalysts.[10] However, as compared to metal surfaces, few[11–15] molecular beam scattering studies have been conducted on metal oxides. Particularly, CO_2 is an ideal probe molecule to map the effect of surface defects, as discussed by Hendersson,[16] Yates,[17] and others. Furthermore, CO_2 is the main source of carbon for hydrogenation surface reactions such as methanol synthesis. In theoretical studies,[18] it has been proposed that oxygen vacancy sites lead to bent CO_2^-, trapped at defect sites which promotes lower energy pathways for subsequent reactions. Thus, the surface as well as the probe molecule chosen for this study is pertinent from a fundamental point of view as well as for industrial applications.

Department of Chemistry, Biochemistry and Molecular Biology, North Dakota State University, Fargo, USA. E-mail: uwe.burghaus@ndsu.edu, www.chem.ndsu.nodak.edu; Fax: 701 231 8831

1.1 Surface defects

Surface defects on TiO_2(110) attracted the interest of many research groups[16,17,19] because surface defects were the active sites, for example, for O_2 and H_2O dissociation[4,20] and metal nanocluster nucleation.[21] Among the different techniques used to generate defects ultra-high vacuum (UHV) annealing above 600 K leads to the most well characterized defects, *i.e.*, oxygen vacancy sites form. According to a study using scanning tunneling microscopy (STM),[22] ion sputtering (500 eV, 2 h) creates "craters" of ~50 Å and a metallization of the surface; atomic resolution was not obtained. Ion sputtering the surface was proposed to remove preferentially surface oxygen.[16,23]

A single CO_2 TDS peak (α_1 peak) appeared on the oxidized surface (at 137 K[16]–150 K[17]) which was assigned to adsorption on fivefold coordinated Ti^{4+} sites[16,18] (which corresponds to 5×10^{14} molecules cm^{-2} at saturation). Annealing at temperatures above 600 K resulted in a second (α_2 peak) high temperature TDS peak (at 166 K[16]–200 K[17]), that was assigned to adsorption on Ti^{3+} oxygen vacancy sites[17] (Fig. 1). (For example, a defect density of 10% would correspond to 5×10^{13} vacancies cm^{-2}). The shape of the TDS curves and the intensity ratio of the peaks depended on the defect density, Γ. Similar effects were revealed recently for CO_2/ZnO(0001).[24] However, as pointed out in ref. 17 a simple quantitative correlation of the α_2 TDS peak intensity and defect density appears very difficult since saturating the surface perfectly with CO_2 was difficult. Annealing above 1100 K can induce reconstruction of (2 × 1) TiO_2(110) which also affects significantly the shape of the CO_2 TDS curves.[17] Thus, CO_2 can be used to study the effect of surface structure on binding energies [kinetic structure–activity relationships (SARs)] for metal oxides. Even the nearly perfect surface consisted, according

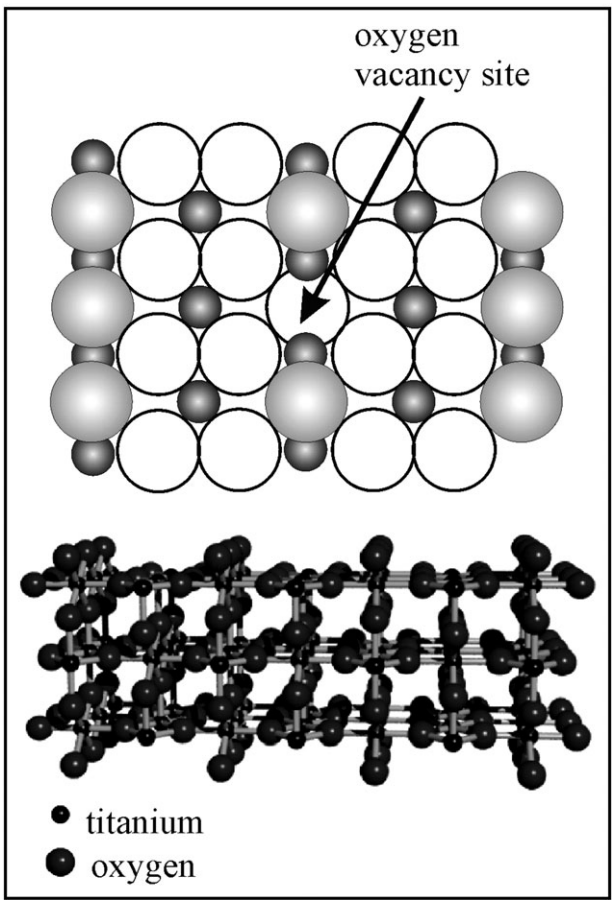

Fig. 1 Schematics of the surface. The top panel shows an overhead view indicating the position of an oxygen vacancy site. The bottom panel is a 3-D view of the surface which suggests that the adsorption of CO_2 is sterically hindered due to the corrugation of the surface.

to STM results,[25] of ~10% oxygen vacancy sites which depended on the history of the sample preparation.

1.2 Dynamics of CO_2 adsorption

Molecular beam scattering experiments with CO_2 have, to the best of our knowledge, been conducted for ZnO(0001), Pt(111), Pd(111), Cu(110) and Ni(100) surfaces.[26–29] Excepting Ni(100), for all of these systems non-dissociative and non-activated molecular adsorption was observed. For all systems at large impact energies and low adsorption temperatures, S(Θ) was dominated by the effect of an extrinsic (trapping above occupied sites) precursor state. An effect of Γ on S(Θ) was observed for CO_2/ZnO(0001)[26] and an anisotropy in S_0 for $CO/TiO_2(110)$,[14] *i.e.*, a dynamic SAR (structure activity relationship) was present. CO_2 adsorption was also studied on a variety of other systems.[30–39]

1.3 Site blocking effects

The term site blocking is commonly assigned to the influence of preadsorbates on the adsorption dynamics of adsorbates. The adsorption dynamics can be mapped by measuring S_0 and S(Θ) of the adsorbate. Pure physical site blocking refers to blocking of special adsorption sites, *i.e.*, competitive adsorption of reactants and preadsorbates. This would lead, in the simplest case, to a decrease in S_0 of the adsorbate with increasing coverage of the pre-adsorbate, simply due to the reduction of sites available for the adsorbate. In contrast, oxygen vacancy sites on $TiO_2(110)$ may, in the simplest case, lead to an increase in S_0 since new adsorption sites for CO_2 form.

A (1 × 1) hydrogen structure was observed[42,43,53] for both $TiO_2(110)$ and ZnO(0001) by dosing with atomic hydrogen. In the latter case, H atoms also etch the surface readily which was not observed for $TiO_2(110)$. On ZnO(0001) hydrogen blocks specifically defect sites,[24] which may provide a tool to identify certain reaction pathways; therefore, H–CO_2 coadsorption experiments are included in the present study. Adsorption of oxygen is known[44] to "heal out" defects on TiO_2. Therefore, O–CO_2 coadsorption experiments are included in the present project as well. O_2 adsorbs molecularly below 150 K and dissociatively above this temperature.[44] Molecular oxygen adsorbed on oxygen vacancy sites and on adjacent Ti sites. One oxygen vacancy site was proposed to anchor up to three O_2 molecules.[44] Above 150 K, O_2 dissociates on defect sites, filling the oxygen vacancy site and one adjacent Ti site. Therefore, the reduction of Γ by O_2 exposure is expected to be associated with the blocking of additional Ti sites on the surface.

In this study, the macroscopic effects of surface defects on the reactivity of the system were characterized using molecular beam scattering and TDS with the final goal being to develop SAR rules. Whereas sputtering and annealing the surfaces leads to an increase in Γ, preadsorption of oxygen and/or hydrogen may decrease Γ. A related study about CO and CO_2 adsorption on defected ZnO(0001) was presented recently;[26,46] the results will be compared with the TiO_2 system studied here. Some results of $CO_2/TiO_2(110)$ were presented elsewhere.[47]

2. Experimental procedures

The measurements were collected using a home-built, triply-differentially pumped molecular beam system.[26] The impact energy, E_i, of the CO_2 molecules were varied within (0.12–1.3) eV by using pure CO_2 and by seeding with 3% or 10% of CO_2 in He, combined with a variation of the nozzle temperature within 300–700 K. According to the reproducibility and the signal-to-noise ratio of the King and Wells[48] curves, the statistical error in S_0 was below ±0.03. The S(Θ) and TDS data were smoothed, conserving, however, the shape of the curves. All adsorption probabilities were obtained for normal impact on the surface. A saturation coverage of 1 monolayer (ML) of CO_2 was assumed for T_s ~ 85 K which is common practice. A number of precautions were taken for the TDS measurements (heating rate of ~1.5 K s^{-1}) to guarantee that the data were not obscured by contributions from the sample holder, as discussed in ref. 49 and 50. The sample was cooled in less than 10 min; a combined TDS–adsorption probability measurement required less than 15 min; the base pressure of the scattering chamber was in the low 10^{-10} mbar range. The reading of the thermocouple was calibrated *in situ* by TDS measurements of *n*-butane assuming a binding energy of 27 kJ mol^{-1} and a 0th order preexponential of 1×10^{28} 1/(s cm^2).[26,51] Atomic hydrogen was generated by dissociation on a hot W-filament (chamber backfilling at 1×10^{-6} mbar through a dosing capillary). Cold traps with dry ice were used.

3. Results

3.1 Characterization of TiO_2(110) samples

The density of defects was qualitatively characterized by TDS as summarized in Fig. 2. An initially transparent crystal was studied (MaTeck) which was cleaned initially by a procedure consisting of approximately 20 cycles of Ar^+ sputtering (600 V, ~4 μA, 30 min, T_s = 300 K) followed by annealing in oxygen (1×10^{-6} Torr, T_s = 600 K, 10 min) and in UHV (T_s = 750 K, 5 min). The procedure was adapted from a prior He Atom Scattering (HAS) study which produced a large He atom reflectivity from the sample[14] suggesting a small Γ.

TDS data of the sample saturated by CO_2 is shown in Fig. 2A. The TDS curve consisted of two peaks at ~134 K and ~176 K labeled as α_1 and α_2. Fig. 2B depicts the saturation coverage, Θ_{sat}, of CO_2 obtained by integrating adsorption transients measured as a function of T_s. The curve consisted of two sections having distinctly different slopes.

3.2 Initial sample preparation

The E_i dependence of the adsorption probability is illustrated in Fig. 3 and the effect of T_s in Fig. 4. The effect of varying the defect density by sputtering and annealing is depicted in Fig. 5; the effect of pre-adsorbates is summarized in Fig. 6.

The initial adsorption probability, S_0, of CO_2 decreased linearly as E_i increased (Fig. 3A). The curve was parameterized using $S_0 = 0.557–0.263\ E_i$ (E_i in eV, solid line in Fig. 3A). This type of parameterization was used in this study, because it is useful[52,53] for developing kinetic models of surface reactions with CO_2 and for comparing results with other systems. Additionally, included in Fig. 3A are results[26,46] for CO_2/ZnO(0001) and CO/ZnO(0001). The general shape of S_0 *vs.* E_i curves appeared to be independent of the surfaces but were related specifically to the probe molecule; for CO an exponential decrease was observed.

$S(\Theta)$ of CO_2 shown in Fig. 3B depended weakly on coverage until the surface was saturated wherein S drops naturally to zero. The (MCS)[40,54] scheme (solid lines in Fig. 3B) used to fit the data included two parameters, S_0 and S_{occu} (see section 4.2). The adsorption probability in the extrinsic precursor state, S_{occu}, as obtained from the fitted data, decreased linearly from 0.40 to 0.18 within E_i = 0.12–1.29 eV obeying the equation $S_{occu} = 0.564 + 0.196\ E_i$ (with E_i in eV). Additionally, the Kisliuk model[55] ($S(\Theta) = S_0\ /[1 + \Theta/(\Theta_{sat} - \Theta)K]$) was applied because it can, as an analytic model, be used easily to compare the data with other systems. Typical examples of Kisliuk fits are depicted as dashed lines in Fig. 3B. The precursor parameter K increased linearly from 0.12 to 0.25 within the E_i range studied ($K = 0.105 + 0.128\ E_i$, E_i in eV). In most cases, slightly better fits were obtained with the MCS.

S_0 was independent of T_s within the impact energy range studied (Fig. 4A). The S_0 values of the $S(\Theta)$ curves parametric

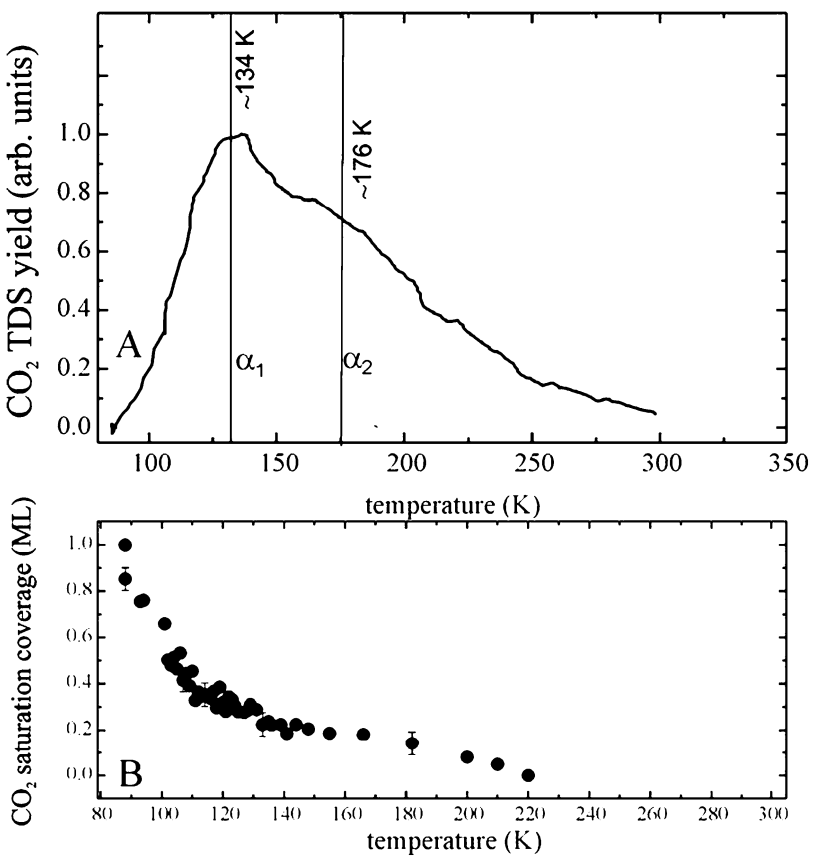

Fig. 2 (A) CO_2 TDS for the surface saturated with CO_2 (heating rate 1.5 K s⁻ec). (B) CO_2 saturation coverage *vs.* adsorption temperature as obtained by integration of King and Wells adsorption transients.

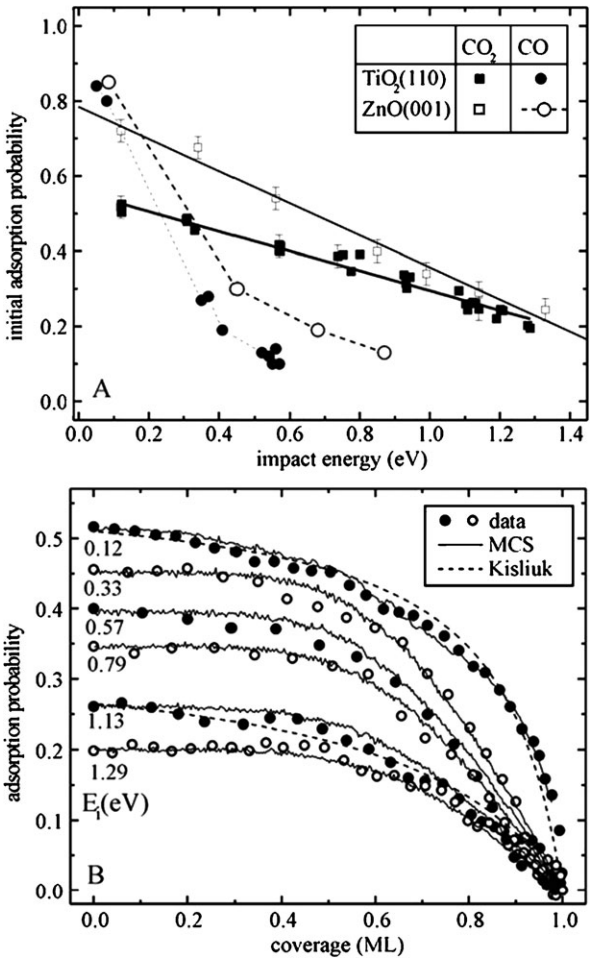

Fig. 3 (A) The initial adsorption probability as a function of impact energy for CO and CO_2 on ZnO(0001) and TiO_2(110) crystals, as indicated. T_s = 85 K, normal impact angle. (B) Coverage dependence of the adsorption probability of CO_2 for TiO_2(110), parametric in impact energy and at constant temperature. The lines resulted from Monte Carlo Simulations (MCS)[41,62] and fits using the Kisliuk model, as indicated.

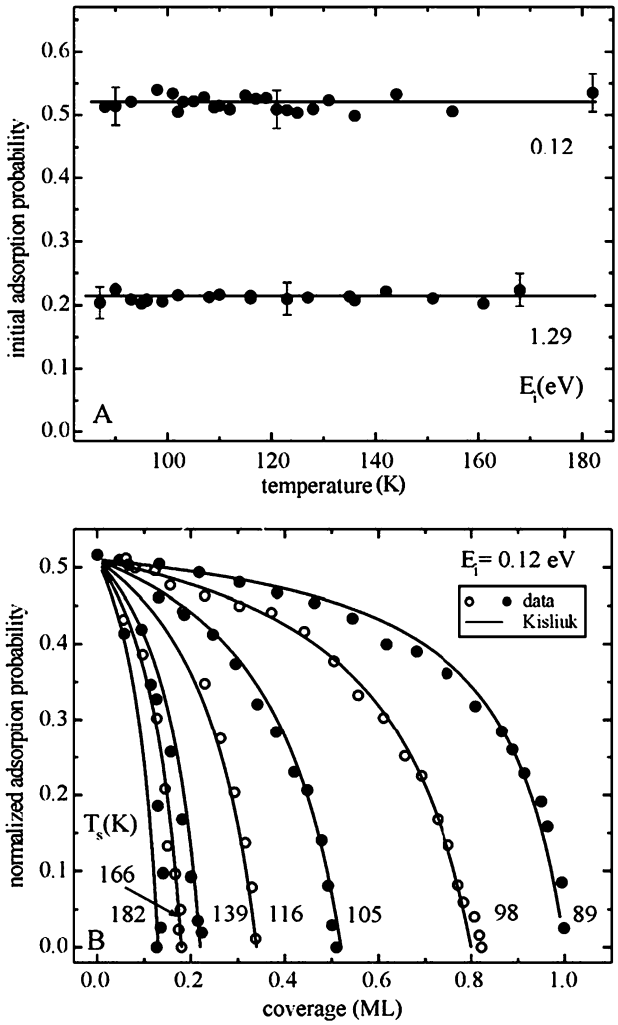

Fig. 4 (A) Temperature dependence of the initial adsorption probability, parametric in impact energy, as indicated, for the initial preparation procedure of the surface. (B) The corresponding coverage dependence of the adsorption probability.

in T_s (Fig. 4B) were normalized to the value obtained by averaging the set of $S_0(T_s)$ curves in Fig. 4A. The saturation coverages, Θ_{sat}, of $S(\Theta)$ for $T_s > 85$ K were normalized with respect to the curve at T_s = 85 K for which Θ_{sat} = 1 ML was assumed, as is common. As T_s increased, the CO_2 saturation coverage naturally decreased (*cf.*, Fig. 2B); the shape of the curves scaled accordingly, *i.e.*, no distinct variations in the $S(\Theta)$ curve shapes were detected by changing T_s. The data were parameterized using the Kisliuk model (solid lines in Fig. 4B); the Kisliuk precursor parameter, K, increased exponentially from 0.12 to 0.32 within 89–180 K ($K = -64.368 \exp(-T_s/15.371) + 0.315$, T_s in K).

3.3 Effect of oxygen vacancy sites on the adsorption dynamics/kinetics

The sample was cleaned using the initial preparation procedure (see section. 3.1). Defects were induced by ion sputtering (600 eV, 85 K, Fig. 5A and 5B) and by annealing ($T > 600$ K, Fig. 5C and 5D) for 1 h under vacuum. In the case of the sputtered surface, the exposure of Ar^+ ions, $\chi(Ar^+)$, were obtained by measuring the sputter current on the sample and were normalized with respect to the surface density[56] (1 ML = 5×10^{15} cm^{-2}).

As $\chi(Ar^+)$ increased, the total CO_2 TDS intensity decreased but interestingly, the α_1 CO_2 TDS peak yield decreased at a faster rate than the α_2 peak (Fig. 5A). Furthermore, S_0 decreased distinctly by ~30% as $\chi(Ar^+)$ increased (Fig. 5B). This observation was in contrast with the results obtained earlier[57] on ZnO(0001).

Consistent with earlier reports,[16,17] the shape of the CO_2 TDS curves changed significantly with annealing temperature (Fig. 5C). As annealing temperature increased, the α_2 peak intensity increased with respect to the α_1 peak intensity. This effect was similar to the results obtained using sputtering (*cf.*, Fig. 5A and 5C), except that the integrated CO_2 TDS intensity increased slightly with annealing time. Although, the data set was limited, it appeared that only for annealing temperatures

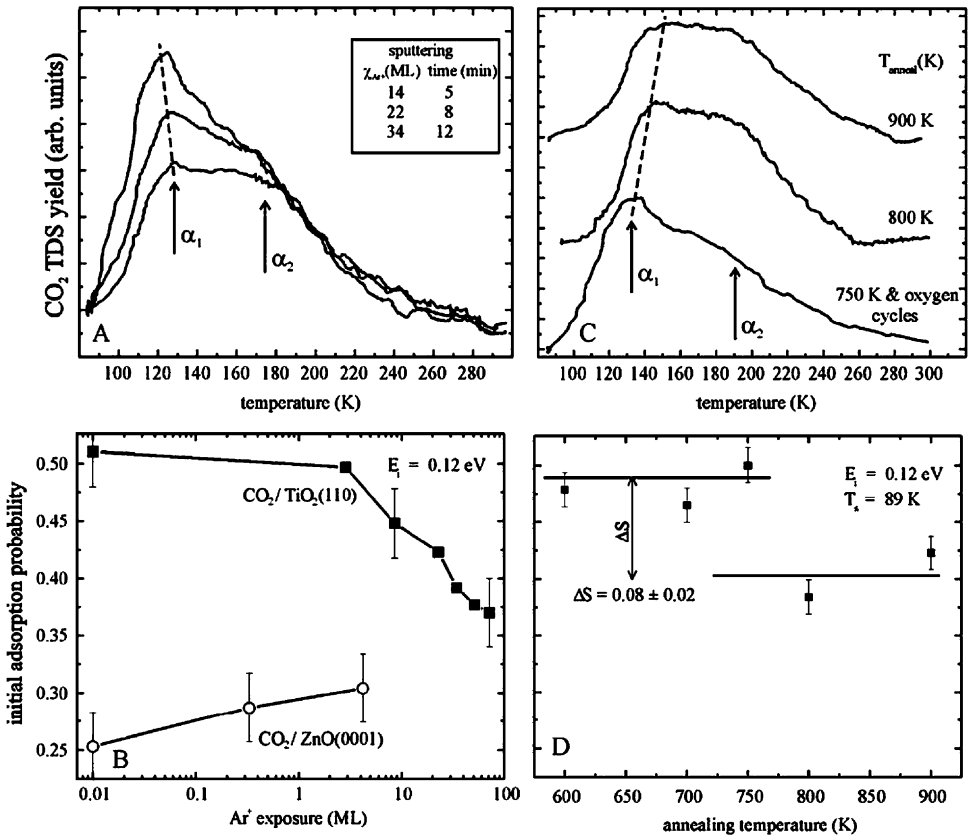

Fig. 5 The increased density of defects generated by (A) and (B) sputtering and (C) and (D) annealing. The top panel shows CO_2 TDS curves of the CO_2 saturated surfaces as a function of Ar^+ exposure and annealing temperature, as indicated. The bottom panel depicts the corresponding S_0 measurements, together with reference data from ref. 37. The TDS curves in C are offset. The lines in D indicate the average of the data points; each data point corresponds to an average of 3–5 independent measurements. Additional parameters A: $T_{sputtering}$ = 85 K, 600 eV, approximately 4 μA.

above 750 K was a decrease (~20%) in S_0 observed (Fig. 5D). Annealing above 900 K was avoided so that reconstruction of the surface was not induced. No significant variation in the S(Θ) curve shapes was detected by either high temperature annealing or sputtering the samples.

3.4 Effect of hydrogen preadsorption on the adsorption kinetics/dynamics of CO_2

The effect of preadsorbed atomic hydrogen on the adsorption of CO_2 was examined for the defected surface using TDS and adsorption probability measurements, as summarized in Fig. 6. The surface was first pre-exposed to hydrogen at ~85 K and saturated subsequently with CO_2 using the molecular beam system. CO_2 TDS curves were then collected (Fig. 6A). The intensity of the TDS curves decreased as H exposure, χ(H), increased while the shape of the curves was approximately conserved.

Other than decreased CO_2 saturation coverage, no significant variation in the S(Θ) curve shapes were produced by preadsorbing hydrogen. However, S_0 of CO_2 decreased exponentially by ~40% as χ(H) increased (Fig. 6B). Data for CO_2—hydrogen coadsorption from a prior study[57] on ZnO(0001) were included. S_0 initially decreased (section (a) in Fig. 6B) as observed for TiO_2(110). However, after 5 min of H exposure, S_0 increased distinctly (section (b) in Fig. 6B) for ZnO(0001). This effect was absent for TiO_2(110).

3.5 Effect of oxygen preadsorption on the adsorption kinetics/dynamics of CO_2

The effect of preadsorbed oxygen contrasts the results obtained for hydrogen, as expected. The following measuring procedure was used. (1) Defects were generated by annealing the surface for 30–60 min at 900 K. (2) Oxygen was preadsorbed. (3) The remaining clean areas of the surface were saturated with CO_2 (at 85 K) by the molecular beam system, while recording simultaneously the adsorption transient. (S_0 obtained from these transients is shown in Fig. 6D.) (4) A CO_2 TDS curve was detected (Fig. 6C). (5) The preadsorbed oxygen was finally desorbed by flashing the surface to 500 K. The procedure (1 to 5) was repeated for different O_2 preexposures, $\chi(O_2)$, at T_{ads} = 250 K and 85 K.

At 0.4–1.0 L of O_2 (at T_{ads} = 85/250 K) the α_2 TDS peak vanished (Fig. 6C). At T_{ads} = 250 K, the intensity of the α_1 TDS peak was conserved, even for large $\chi(O_2)$; at T_{ads} = 85 K (TDS not shown) an increase of the α_1 TDS peak was detected for large $\chi(O_2)$. Although a stabilization of CO_2 by H_2O adsorption was observed in an earlier study,[16] a background effect of H_2O was unlikely because cold traps were used in the gas line and the hydrogen and atomic oxygen coadsorption

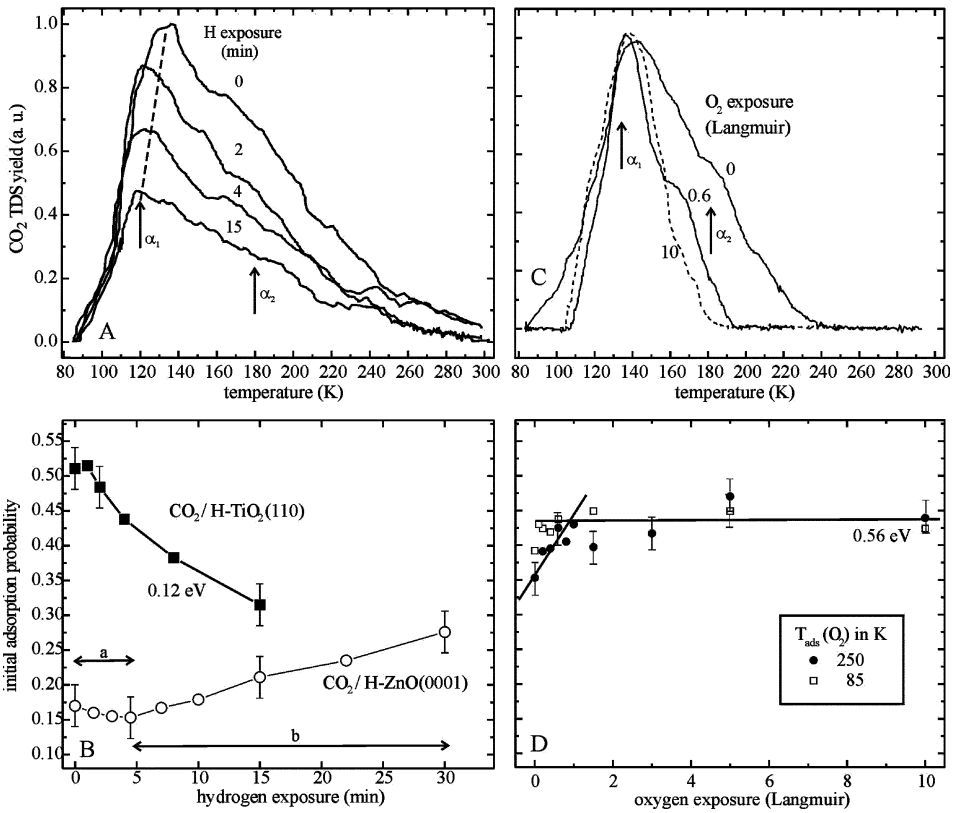

Fig. 6 Coadsorption of atomic hydrogen or oxygen and CO_2 on a defected TiO_2(110) surface. (A) CO_2 TDS as a function of H preexposure (1×10^{-6} torr backfilling, hot-filament dosing capillary, T_s = 85 K). The surface was always saturated with CO_2. (B) Corresponding S_0 of CO_2 on H predosed surface and reference data from ref. 57. (C) CO_2 TDS as a function of O_2 pre-exposure (T_{ads} = 250 K). (D) Corresponding S_0 of CO_2 on O_2 predosed surface parametric in O_2 adsorption temperature.

data did not reveal this effect. Therefore, the stabilization of CO_2 resulting from a large coverage of molecularly adsorbed oxygen is tentatively concluded.

S_0 is illustrated in Fig. 6D as a function of $\chi(O_2)$ and parametric in O_2 adsorption temperature, T_{ads}. S_0 for the clean surface was determined to be smaller than the values reported in Fig. 3A because defects were generated by annealing the surface (*cf.*, Fig. 5D). However, it was very difficult to obtain identical Γ (as quantified by CO_2 TDS) of the sample for different experiments. However, oxygen pre-exposures produced, in all cases, a small but reproducible increase in S_0. The increase was slightly larger for T_{ads} = 250 K than for T_{ads} = 85 K.

4. Discussion

4.1 Sample characterization

The α_1 and α_2 peaks observed in CO_2 TDS curves were assigned to Ti^{4+} (pristine) sites and Ti^{3+} oxygen vacancy sites, respectively (see section 1, Fig. 1). The observation in this study that the α_2 peak intensity increased with respect to the intensity of the α_1 peak using sputtering (Fig. 5A) and annealing the samples (Fig. 5C), as well as the observation of quenching of the α_2 peak with increased $\chi(O_2)$, (Fig. 6C) are in agreement with earlier findings.[16,17] The CO_2 saturation coverage *vs.* adsorption temperature curves (Fig. 2B) also showed two different regimes. Thus, CO_2 TDS curves can be used to qualitatively estimate the density of oxygen vacancy sites on TiO_2. The large α_2 peak intensity indicated a large Γ. Very similar CO_2 TDS curves were recently observed for ZnO(0001), suggesting that this approach can be applied more rigorously to a variety of metal oxide surfaces. Other probe molecules revealed similar trends.[58] However, the rather large binding energies of CO_2 on metal oxides (as compared with metals), makes CO_2 a particularly well suited probe molecule for sampling surface defects. It appears essential to always characterize Γ when studying TiO_2. A simple and convenient procedure, outlined earlier,[16,17,20] was CO_2 TDS. Local imaging techniques such as STM are difficult to apply to strongly reduced samples. Therefore, automically resolved STM data on highly defected TiO_2 surfaces are not available.[45] However, defects can affect significantly the catalytic performance of metal oxides.

4.2 Adsorption dynamics and kinetics on slightly reduced samples

4.2.1 Kinetics. The binding energy of CO_2 adsorbed on pristine and defect sites amounted to $\sim$36 kJ mol^{-1} and 48 kJ mol^{-1}, respectively, as estimated from the TDS peak temperatures using the Redhead equation (pre-exponential factor[17] =

4×10^{13} s^{-1}). Depending on the day-to-day reproducibility (±5 K) of the TDS peak positions, an uncertainty of ±2 kJ mol^{-1} was estimated. The small absolute shift of the TDS peak temperatures to lower temperatures, as compared with ref. 17 may be related to uncertainties in the temperature measurement rather than the larger Γ of our sample because the onset of the α_1 structure shifted by approximately 10 K to larger temperatures as Γ increased (see dashed lines in Fig. 5A/C). The TDS data were not analyzed with more sophisticated techniques because the results were in agreement with previous findings; the TDS was applied in this study to correlate qualitatively the surface structure with the adsorption dynamics of CO_2.

4.2.2 Dynamics. The decrease in S_0 observed with increasing E_i (Fig. 3A) indicated molecular and non-activated adsorption. The decrease resulted from the requirement to dissipate larger amounts of kinetic energy of the gas phase species to the surface with increasing E_i in order to adsorb. Thus, the adsorption process becomes less likely at large E_i. In contrast, for activated and dissociative adsorption, an increase in S_0 would be expected above a given threshold energy.

Within the impact energy range studied, the shape of $S(\Theta)$ was in agreement with precursor-mediated adsorption, as predicted by the Kisliuk model[55,59] (see dashed lines in Fig. 3B). Accordingly, particles which targeted adsorption sites already blocked were trapped in an extrinsic precursor state. The lifetime of the precursor state was, at low T_s, long enough such that the trapped particles diffused with a large probability to empty sites before the particles desorbed. Therefore, $S(\Theta)$ remained constant until the surface was saturated. For direct adsorption, without the effect of precursor states, $S(\Theta)$, according to Langmuirian adsorption dynamics, would decrease linearly.

The MCSs[40,54] adopted the idea of the Kisliuk model. The MCSs quantified the trapping probability into the precursor state which decreased by a factor of two as E_i increased, consistent with the results obtained with the Kisliuk model. The Kisliuk parameter, K, is inversely related to the trapping probability. The smaller the value of K, the larger is the effect of the precursor states. MCSs are a more direct approach to quantify trapping probabilities.

S_0 was independent of T_s (Fig. 4A) which supported the conclusion of molecular and non-activated adsorption. The shape of the $S(\Theta)$ curves was fully consistent with non-activated and precursor-mediated adsorption. The decrease in Θ_{sat} with T_s, as shown in Fig. 2B and 4B, was the result of a CO_2 adsorption/desorption equilibrium. During the adsorption probability measurements, the adsorption was driven by the impinging flux of CO_2 molecules. As T_s approached the desorption temperature, Θ_{sat} decreased because of thermal desorption. The MCS scheme used does not include temperature effects. Therefore, the Kisliuk model was applied to parameterize the data of Fig. 4B. The increase in K with T_s reflected the decreasing lifetime of CO_2 in the precursor state as T_s increased.

The Γ affected S_0 (*cf.*, Fig. 3A) but did not affect significantly the shape of the adsorption probability curves. Thus, the extrinsic precursor dynamics of CO_2 on TiO_2(110) was little affected by oxygen vacancy sites. However, results obtained on a sputtered Cu(110) surface where the shape of the $S(\Theta)$ curve was also dependent on Γ[60] demonstrated that this is not always the case. The decrease in S_0 with increasing Γ (Fig. 2A) suggests changes, for example, of the lattice force constants and the CO_2-to-surface mass-match at the point of impact.

4.3 Adsorption dynamics and kinetics on strongly reduced samples

The increased α_2 TDS intensity with respect to the α_1 peak intensity as $\chi(Ar^+)$ (Fig. 5A) and annealing temperatures increased (Fig. 5C) was consistent with the expected increase in Γ. Generating defects by annealing required large temperatures (Fig. 5C), in agreement with earlier findings.[17]

The shape of the TDS curves obtained by the two different (sputtering/annealing) procedures was similar. For example, compare the TDS curves obtained at 34 ML Ar^+ exposure and 900 K annealing (Fig. 5A/C). Furthermore, the α_1 peak position shifted slightly to larger temperatures with increasing Γ in both cases. This observation suggested that, as proposed before,[23] oxygen atoms were preferentially sputtered; or, that sputtering led to a local chemical environment of the catalytically active areas on the sample that was quite similar to the one obtained by annealing in vacuum. Furthermore, sputtering and annealing led to approximately the same absolute magnitude of the decrease in S_0. This result may be expected because the shape of the final TDS curves, in each of the data sets of the annealing/sputtering experiments, were quite similar (see Fig. 5A/C).

However, sputtering decreased Θ_{sat}, *i.e.*, the total TDS peak area decreased with $\chi(Ar^+)$ (Fig. 5A). Thus, surface areas inactive towards CO_2 adsorption were formed that may correspond to the craters and the onset of metallization of the surface observed in an STM study[22] on sputtered surfaces. Note that the CO_2 binding energy on metal surfaces such as Cu(110) is often smaller (desorption temperature 90 K) than on metal oxides.[28]

In the simplest case, an increase in S_0 would be expected with increasing density[40] of oxygen vacancy sites since new Ti sites, *i.e.*, adsorption sites for CO_2, should form. However, the experimental evidence contradicted this simple model. The adsorption of CO_2 on oxygen vacancy sites may be sterically hindered (Fig. 1) which would reduce the probability of this process. Thus, S_0 would decrease with increasing annealing time, as was observed (Fig. 5D). In the case of the sputtered surface, additional, more complicated defects (kinks, step edges, terraces, *etc.*) formed which were not active towards CO_2 adsorption since S_0 and the saturation coverage decreased.

Interestingly, defects obtained by sputtering another metal oxide such as ZnO(0001) showed the opposite trend (Fig. 5B and ref. 26). Sputtering conserved the termination of ZnO surfaces. For ZnO(0001), oxygen-terminated step edges were related to the intrinsic defect structures.[61] Thus, the number of step edges should increase with increasing sputtering time. The adsorption along these sites should not be sterically hindered which explains the differences observed in the reactivity of sputtered TiO_2 and ZnO surfaces.

Although defects were identified as the active sites for bond breaking processes (O_2, H_2O adsorption), they obviously reduced the reactivity for molecular adsorption processes such as CO_2 on TiO_2(110). S_0 is a macroscopic property. Therefore, the adsorption probability on different sites cannot directly and easily be distinguished experimentally. The rather small effect on S_0 with defect density is expected since the behavior of only a part of the surface is modified. Thus, even if the local effect on the adsorption dynamics is very large the variations in the total (measured) adsorption probabilities will be rather small. Therefore, we can conclude that the local effect of defects on the adsorption dynamics will be significantly larger than the observed variations in the total S_0 values. Obtaining more quantitative results is hampered by a precise determination of the defect density which would be required for, *e.g.*, Monte Carlo simulations.

4.4 Effect of hydrogen adsorption on defected samples

CO_2 adsorption data were collected for TiO_2(110) preadsorbed with hydrogen or oxygen. Interestingly, different metal oxides behave quite differently. In a previous study about H/ZnO(0001), preferential blocking of defect sites by atomic hydrogen was observed by TDS[57] which was accompanied by a decrease in S_0 as expected for physical site blocking (section (a) in Fig. 6B). S_0 naturally decreased with increasing H pre-exposure because the number of available adsorption sites for CO_2 adsorption decreased. However, exposure of large amounts of atomic H on ZnO increased the defect density (H etching) as observed in HAS. In this exposure regime, S_0 increased with H exposure (section (b) in Fig. 6B) which was consistent with the increase in S_0 observed on sputtered ZnO(0001) (open circular points in Fig. 6B).

In contrast to CO_2 TDS[24] on ZnO and according to the TDS data (Fig. 6A) for H/TiO_2(110), H did not block specifically oxygen vacancy sites on TiO_2(110). The intensity of both TDS peaks decreased as χ(H) increased (Fig. 6A).

The decrease in S_0 as χ(H) decreased indicated simply, as in the case of ZnO(0001), a physical site blocking for TiO_2(110). This process competed, in the case of ZnO(0001), with an etching of the surface by H, which interestingly, was absent for TiO_2(110). Indeed, a HAS study[42] revealed the formation of an ordered H overlayer on TiO_2(110) without a breakdown of the outermost surface layer, even for large H exposures. A small shift ($\sim$10 K) of the onset of the TDS peaks to smaller temperatures as χ(H) increased, indicated a weak ($\sim$4 kJ mol^{-1}) repulsive H–CO_2 interaction on TiO_2(110).

4.5 Effect of oxygen adsorption on defected samples

In consideration of the results of previous studies,[16,17] and the decrease in S_0 with increasing Γ (Fig. 5D) observed here, a variation in S_0 depending on $\chi(O_2)$ was expected. However, oxygen did not only "heal out" oxygen vacancy sites, it also produced blocking of additional Ti sites (section 1.3). In the former case, S_0 should increase due to the decrease in Γ (*cf.*, Fig. 5D), but this effect competes with an expected decrease in S_0 due to the blocking of Ti sites. Thus, rather small overall effects on S_0 are expected. Indeed, a small increase in S_0 with increasing $\chi(O_2)$ was observed (Fig. 6D) which illustrated again that the reactivity of the surface was correlated with the Γ. The increase in S_0 was accompanied by the vanishing of the α_2 TDS (defect) peak (Fig. 6C), indicating that the oxygen vacancy sites "heal out". The effect of $\chi(O_2)$ on S_0 (Fig. 6D) was slightly smaller than the annealing effect (Fig. 5D) consistent with a competition of the reduction of Γ and the blocking of CO_2 adsorption sites by oxygen. The effect of molecularly adsorbed O_2 on S_0 was slightly smaller than the effect of atomic oxygen (Fig. 6D) which is in qualitative agreement with the model that one oxygen vacancy site leads to three adsorbed O_2 molecules.[44] Thus, the site blocking effect of molecularly adsorbed oxygen should be larger than for atomically adsorbed oxygen. However, it is very difficult to maintain an identical initial state of the surface throughout the project.

5. Summary

The density of oxygen vacancy sites, Γ, on TiO_2(110) was correlated qualitatively with the reactivity of CO_2 adsorption. Whereas kinetic SARs (structure activity relationship) were frequently observed, systematic investigation of the effect of defects on gas-surface energy transfer processes (dynamic SARs) are rather rare. CO_2 thermal desorption spectroscopy (TDS) was applied to characterize qualitatively the Γ parameter. In agreement with prior studies, two structures were detected; a single TDS peak (α_1) was observed for a fully oxidized surface[17] whereas large intensities of a second TDS peaks (α_2) indicated a large Γ.

- Non-activated, precursor mediated, adsorption dynamics were observed independently to the value of Γ. Monte Carlo simulations (MCSs) and the Kisliuk model were used to parameterize the data and to quantify the trapping probability into the extrinsic precursor state.
- The shape of CO_2 TDS curves depended on Γ and the coverage of (O_2, H_2) preadsorbates. Thus, a kinetic SAR was observed.
- Oxygen vacancy sites decreased the initial reactivity, S_0, toward CO_2 adsorption. Thus, a dynamic SAR was observed.
- According to the TDS results, oxygen adsorption produced a reduction of Γ. S_0 increased with increasing oxygen pre-exposure on a defected surface.
- H preadsorption induced physical site blocking. S_0 decreased as H coverage increased.
- Ion sputtering and annealing the surface increased Γ and produced similar chemical behavior of the surface toward CO_2 adsorption.
- Only small effects on the macroscopic S_0 values (determined experimentally) can be expected even if the local effect of defects on the adsorption dynamics is large, as was consistent with the experimental findings.

Acknowledgements

Acknowledgment is made to "The Donors of the American Chemical Society Petroleum Research Fund" (type G) for partial financial support. Assistance by B. Hokkanen and E. Johnson in the beginning stages and by T. Nurkic in the final stages of the project is acknowledged.

References

1 M. Haruta, *Catal. Today*, 1997, **36**, 153.
2 T. V. Choudhary and D. W. Goodmann, *Top. Catal.*, 2002, **21**, 25.
3 A. L. Linsebigler, G. Lu and J. T. Yates, *Chem. Rev.*, 1995, **95**, 735.
4 M. A. Henderson, *Surf. Sci. Rep.*, 2002, **46**, 1.
5 A. Alvarez, A. J. Fort and E. Bernabeu, *Thin Solid Films*, 1999, **349**, 212.
6 H. Li, A. Khor and P. Cheang, *Biomaterials*, 2002, **23**, 85.
7 C. L. Huisman, A. Goossens and J. Schoonman, *Chem. Mater.*, 2003, **15**, 4617.
8 M. Penza, C. Martucci and G. Cassano, *Sens. Actuators, B*, 1998, **50**, 52.
9 S. Y. Huang, L. Kavan, I. Exnar and M. Graetzel, *J. Electrochem. Soc.*, 1995, **142**, L142.
10 P. A. Cox, *Transition metal oxides*, Clarendon Press, Oxford, 1995.
11 C. R. Henry, *Surf. Sci. Rep.*, 1998, **31**, 235.
12 D. Brinkley, M. Dietrich, T. Engel, P. Farrall, G. Ganter, A. Schafer and A. Szuchmacher, *Surf. Sci.*, 1998, **395**, 292.
13 T. Becker, C. Boas, U. Burghaus and C. Wöll, *Phys. Rev. B*, 2000, **61**, 4538.
14 M. Kunat and U. Burghaus, *Surf. Sci.*, 2003, **544**, 170.
15 J. Libuda, *Surf. Sci.*, 2005, **587**, 55–68.
16 M. A. Henderson, *Surf. Sci.*, 1998, **400**, 203.
17 T. L. Thompson, O. Diwald and J. T. Yates, *J. Phys. Chem. B*, 2003, **107**, 11700.
18 S. A. French, A. A. Sokol, S. T. Bromley, C. R. A. Catlow, S. C. Rogers, F. King and P. Sherwood, *Angew. Chem.*, 2001, **40**, 4437.
19 W. Göpel, G. Rocker and R. Feierabend, *Phys. Rev. B*, 1983, **28**, 3427.
20 M. A. Henderson, *Surf. Sci.*, 1994, **319**, 315.
21 B. K. Min, W. T. Wallace and D. W. Goodman, *Surf. Sci.*, 2006, **600**, L7.
22 Q. Zhong, J. M. Vohs and D. A. Bonnell, *Surf. Sci.*, 1992, **274**, 35.
23 M. A. Henderson, *Surf. Sci.*, 1999, **419**, 174.
24 J. Wang and U. Burghaus, *Chem. Phys. Lett.*, 2005, **403**, 42–46.
25 S. Wendt, R. Schaub, J. Matthiesen, E. K. Vestergaard, E. Wahlström, M. D. Rasmussen, P. Thostrup, L. M. Molina, E. Lægsgaard, I. Stensgaard and F. Besenbacher, *Surf. Sci.*, 2005, **598**, 226.
26 J. Wang and U. Burghaus, *J. Chem. Phys.*, 2005, **122**, 044705–11.
27 C. L. Kao, A. Carlsson and R. J. Madix, *Surf. Sci.*, 2002, **497**, 356.
28 S. Funk, B. Hokkanen, J. Wang, U. Burghaus, G. H. Bozzolo and J. E. Garces, *Surf. Sci.*, 2006, **600**, 583–590.
29 M. P. D'Evelyn, A. V. Hamza, G. E. Gdowski and R. J. Madix, *Surf. Sci.*, 1986, **167**, 451–473.
30 P. J. Moller, S. A. Komolov, E. F. Lazneva and E. H. Pedersen, *Surf. Sci.*, 1995, **323**, 102.
31 J. B. Martins, E. Longo and C. A. Taft, *Int. J. Quantum Chem.*, 1998, **70**, 367.
32 W. Goepel, R. S. Bauer and G. Hansson, *Surf. Sci.*, 1980, **99**, 138.
33 H. Kuhlenbeck, C. Xu, B. Dillmann, M. Haßel, B. Adam, D. Ehrlich, S. Wohlrab, H. J. Freund, U. A. Ditzinger, H. Neddermeyer, M. Neuber and M. Neumann, *Ber. Bunsen-Ges. Phys. Chem.*, 1992, **96**, 15.
34 H. J. Freund and M. W. Roberts, *Surf. Sci. Rep.*, 1996, **25**, 225.
35 J. Nerlov, S. V. Hoffmann, M. Shimomura and P. J. Moller, *Surf. Sci.*, 1998, **401**, 56.
36 S. Funk, B. Hokkanen, J. Wang, U. Burghaus, G. H. Bozzolo and J. E. Garces, *Surf. Sci.*, 2005, **600**, 1870–1876.
37 J. Wang, S. Funk and U. Burghaus, *J. Chem. Phys.*, 2005, **123**, 204710.
38 K. H. Ernst, D. Schlatterbeck and K. Christmann, *Phys. Chem. Chem. Phys.*, 1999, **1**, 4105.
39 J. Onsgaard, S. V. Christensen, P. J. Godowski, J. Nerlov and S. Quist, *Surf. Sci.*, 1997, **370**, L137.
40 J. Stephan and U. Burghaus, *Surf. Sci.*, 2002, **507–510**, 736.
41 U. Burghaus, J. Stephan, J. M. Rogowska and L. Vattuone, *A Practical Guide to Monte Carlo Simulations And Classical Molecular Dynamics Simulation—An Example Book*, NOVA science, New York, USA, 2006, ISBN 1-59454-531-6.
42 M. Kunat, U. Burghaus and C. Wöll, *Phys. Chem. Chem. Phys.*, 2004, **6**, 4203–4207.
43 T. Becker, S. Hövel, C. Boas, M. Kunat, U. Burghaus and C. Wöll, *Surf. Sci.*, 2001, **486**, L502.
44 M. A. Henderson, W. S. Epling, C. L. Perkins, C. H. Peden and U. Diebold, *J. Phys. Chem. B*, 1999, **103**, 5328.
45 A. Szabo and T. Engel, *Surf. Sci.*, 1995, **329**, 241.
46 T. Becker, M. Kunat, C. Boas, U. Burghaus and C. Wöll, *J. Chem. Phys.*, 2000, **113**, 6334.
47 S. Funk, B. Hokkanen, E. Johnson and U. Burghaus, *Chem. Phys. Lett.*, 2006, **422**, 461–465.
48 D. A. King and M. G. Wells, *Surf. Sci.*, 1972, **29**, 454.
49 J. Wang and U. Burghaus, *J. Chem. Phys.*, 2005, **123**, 184716.
50 J. Wang, B. Hokkanen and U. Burghaus, *Surf. Sci.*, 2005, **577**, 158–166.
51 C. Xu, B. E. Koel and M. T. Paffett, *Langmuir*, 1994, **10**, 166.
52 T. S. Askgaard, J. K. Norskov, C. V. Ovesen and P. Stoltze, *J. Catal.*, 1995, **156**, 229.
53 U. Burghaus, J. Ding and W. H. Weinberg, *Surf. Sci.*, 1998, **396**, 273.
54 U. Burghaus, *Surf. Rev. Lett.*, 2001, **8**, 353.
55 P. Kisliuk, *J. Phys. Chem. Solids*, 1957, **3**, 95.
56 L. Vattuone, L. Savio and M. Rocca, *Chemisorption dynamics in the presence of well defined, surface defects, Series in Surface Chemistry: Surface, Dynamics*, ed. D. P. Woodruff, Elsevier, Amsterdam, 2003.
57 J. Wang and U. Burghaus, *Surf. Rev. Lett.*, 2004, **11**, 521–529.
58 A. Linsebigler, L. Guangquan and J. T. Yates, *J. Chem. Phys.*, 1995, **103**, 9438.
59 P. Kisliuk II, *J. Phys. Chem. Solids*, 1958, **5**, 78.
60 U. Burghaus, *Surf. Rev. Lett.*, 2003, **10**, 7.
61 O. Dulub, U. Diebold and G. Kresse, *Phys. Rev. Lett.*, 2003, **90**, 016102.
62 J. Stephan and U. Burghaus, *J. Vac. Sci. Technol., A*, 2003, **21**, 1284.